Progress In Electromagnetics Research, Vol. 137, 239–254, 2013

AN ULTRA-LOW LOSS SPLIT RING RESONATOR BY SUPPRESSING THE ELECTRIC DIPOLE MOMENT APPROACH

Lei Zhu[1, 2] †, Fanyi Meng[1] †, Fang Zhang[1], Jiahui Fu[1], Qun Wu[1, *], Xumin Ding[1], and Joshua L.-W. Li[3, 4]

[1]Department of Microwave Engineering, Harbin Institute of Technology, Harbin 150001, China

[2]Communication and Electronics Engineering Institute, Qiqihar University, Qiqihar 161006, China

[3]Institute of Electromagnetics and School of Electronic Engineering, University of Electronic Science and Technology of China, Chengdu 611731, China

[4]School of Engineering/Department of Electrical & Computer Systems Engineering, Monash University, Sunway/Clayton, Selangor 46150/Victoria 3800, Malaysia/Australia

Abstract—We propose an effective way to realize the ultra-low loss in a split ring resonator (SRR) by suppressing the electric dipole moment approach. To tremendously reduce the loss, the loss mechanism of the SRR is theoretically analyzed in detail. The nonuniform current distribution on the SRR loop results in the residual electric dipole moment and thus brings the high radiation losses. Three different SRR configurations that the lumped capacitor, the distributed capacitor and the dielectric medium are incorporated into the SRR metamaterial are conceived, by which the uniform current distribution can be observed. This leads to in a finite bandwidth deviated from the resonance frequency where the SRR's loss performance dramatically improves owing to suppression of the residual electric dipole moment. The proposed the loss reduction mechanism has potential applications in negative and zero index metamaterials, especially at THz frequencies and in the optical regime.

Received 17 December 2012, Accepted 12 February 2013, Scheduled 19 February 2013

* Corresponding author: Qun Wu (qwu@hit.edu.cn).

† Lei Zhu and Fanyi Meng have made the same contribution on this paper.

1. INTRODUCTION

Negative index metamaterials (NIMs) have attracted great attention due to their fascinating electromagnetic (EM) properties such as perfect lens, near-field imagings, cloakings, reversal of the Doppler effects, and so on [1–15]. A well-established route of constructing NIM structures is based on the Veselago's theory of left-handed materials (LHM), simultaneous negative permittivity and permeability [16]. However, the negative permittivity and permeability produced by electromagnetic resonance can bring about a very high loss [17, 18]. Reducing the losses is critical for many applications expected from the NIM technology, including perfect lenses, electromagnetic cloaks, and so on.

Therefore, a number of diverse strategies have been proposed toward overcoming the issue of high losses in metamaterials. Achieving such reduction of losses by geometric tailoring of the metamaterial designs appears to be out of reach [19–21]. Optimizing low loss NIMs by using intelligent algorithms has also been proposed [22, 23]. Although these NIMs show the low loss property, this method is not universal and systematic. Another promising and generic approach is to incorporate gain materials into metamaterial designs for compensating their overall losses [24–26]. This approach is very promising and has been theoretically predicted that it can achieve zero-loss metamaterials, even over a broad bandwidth. However, it may not always be possible to find a suitable material to provide the necessary gain at a desired frequency regime. So far, the electromagnetically induced transparency (EIT) effects have been introduced to the metamaterial designs for suppressing the radiation losses [27–36]. Although the losses of the EIT-like metamaterials are very low, they do not maintain the negativity in the real part of constitutive parameters [27, 29, 33, 35]. Tsakmakidis et al. have achieved the low loss and negative permeability metamaterial using the EIT-like effect, but its bandwidth is extremely narrow and this EIT-like structure is not convenient for fabrication due to involving to two different metals [37].

The split ring resonator (SRR) used by Ref. [37] is a very common design to achieve the negative permeability when the H field is normal to the SRR plane [16, 17]. Taking this SRR as an example, this paper proposes an effective approach to obtain the ultra-low loss magnetic metamaterial. The loss mechanism of the SRR is theoretically analyzed in detail. Analytical results indicate that the nonuniform current distribution on the SRR loop results in the residual electric dipole moment and thus brings the high radiation losses. In

order to reduce these losses, the residual electric dipole moment should be greatly suppressed, by which the uniform current distribution can be observed. Therefore, three different SRR configurations that the lumped capacitor, the distributed capacitor and the dielectric medium are incorporated into the existing SRR's cell are proposed, and we study their validity in loss reduction in numerical simulation. Simulation results show that, owing to suppression of the residual electric dipole moment, the SRRs with lumped capacitor, distributed capacitor and dielectric medium exhibit the low loss property.

2. LOSS MECHANISMS FOR THE SRR

We start our analysis by considering a periodic arrangement of a single SRR [37], as shown in Fig. 1(a). The SRRs in Figs. 1(a)–(c) are constructed on the FR4 substrate with a dielectric constant of 4.4, a loss tangent of 0.005 and a thickness of 1 mm, and the material of the metallic SRR is copper with a electric conductivity of 5.96×10^7 S/m and the thickness of 0.018 mm. The incident wave propagates along the z axis paralleling to the SRR plane. E-fields polarized along the y axis and H-fields polarized along the x axis are employed. The exact geometry parameters of the unit cell for the SRR as revealed in Figs. 1(a)–(c) are $a_1 = 5$ mm, $b_1 = 5$ mm, $l_1 = 4.4$ mm, $l_2 = 2$ mm, $l_3 = 0.27$ mm, $s_1 = 1$ mm, $s_2 = 0.3$ mm, $s_3 = 0.03$ mm, $w_1 = 0.3$ mm and $w_2 = 0.03$ mm, respectively. Fig. 1(d) displays the unit cell of the THz SRR with dielectric medium. The geometric parameters of the SRR at THz frequencies are given in the caption of Fig. 1. Along the unit cell boundaries in x and y directions, periodic boundary conditions are enforced to simulate the infinite periodic structure. All numerical simulations are based on the CST MICROWAVE STUDIO.

When the size of the SRR unit cell is much smaller than the wavelength of the incident wave ($l/\lambda \approx 0.055$), the SRR metamaterials can be treated as a homogenous medium according to the effective medium theory. Consequently, the effective permeability of the SRR can be retrieved by employing the method proposed by Ref. [38]. Worth noting that the extraction method of effective parameters proposed by Ref. [38] is available only for the dominant wave mode. Higher order mode interaction of neighbored unit-cells is not taken into account. The effective permeability of the SRR as a function of the normalized frequency $(f - f_0)/f_0$ (f_0 is the magnetic resonance frequency) is plotted in Fig. 2(a). One can see that the negative permeability effect appears near the resonance frequency and the imaginary part of the permeability is very large, which means that the losses of the SRR are very high. It needs to specially point

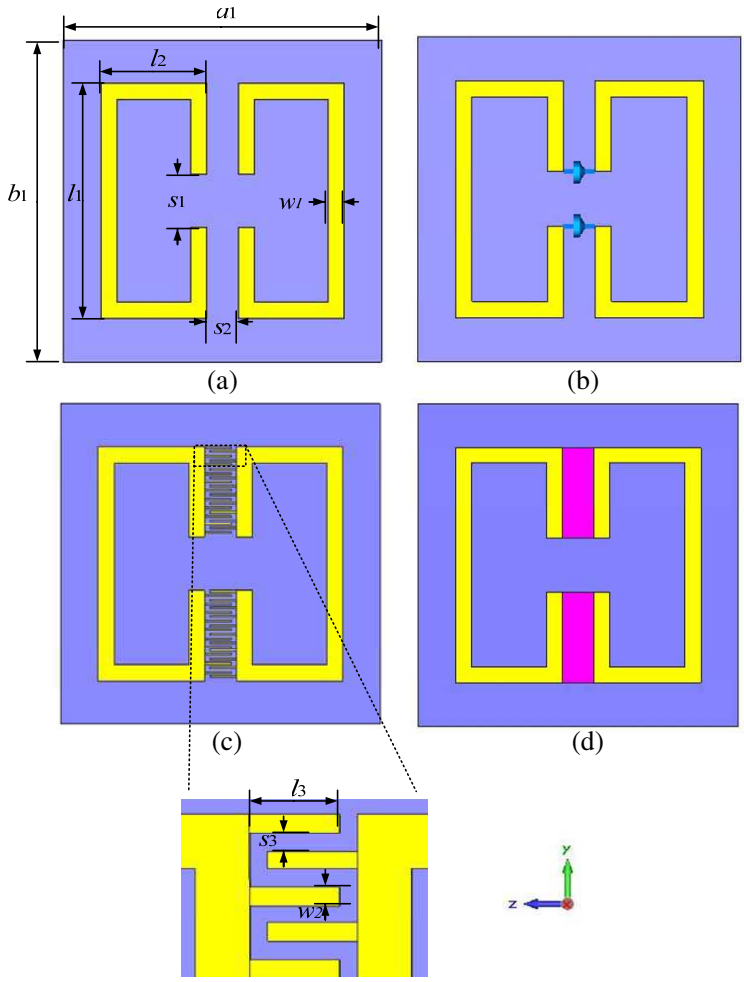

Figure 1. (a) One unit cell of the SRR. (b) One unit cell of the SRR with lumped capacitor. (c) One unit cell of the SRR with interdigital capacitors. The dimensions are $a_1 = 5\,\text{mm}$, $b_1 = 5\,\text{mm}$, $l_1 = 4.4\,\text{mm}$, $l_2 = 2\,\text{mm}$, $l_3 = 0.27\,\text{mm}$, $s_1 = 1\,\text{mm}$, $s_2 = 0.3\,\text{mm}$, $s_3 = 0.03\,\text{mm}$, $w_1 = 0.3\,\text{mm}$, and $w_2 = 0.03\,\text{mm}$. (d) One unit cell of the SRR with dielectric medium. The geometric parameters of the SRR at THz frequencies are $a_1 = 60\,\mu\text{m}$, $b_1 = 60\,\mu\text{m}$, $l_1 = 50\,\mu\text{m}$, $l_2 = 22\,\mu\text{m}$, $s_1 = 10\,\mu\text{m}$, $s_2 = 6\,\mu\text{m}$, and $w_1 = 3\,\mu\text{m}$. The thicknesses of the substrate glass (ε_r of 4.84 and a loss tangent of 0.0054) and the metal copper are 10 µm and 8 µm, respectively. The ε_r of the dielectric medium (magenta) is 11.

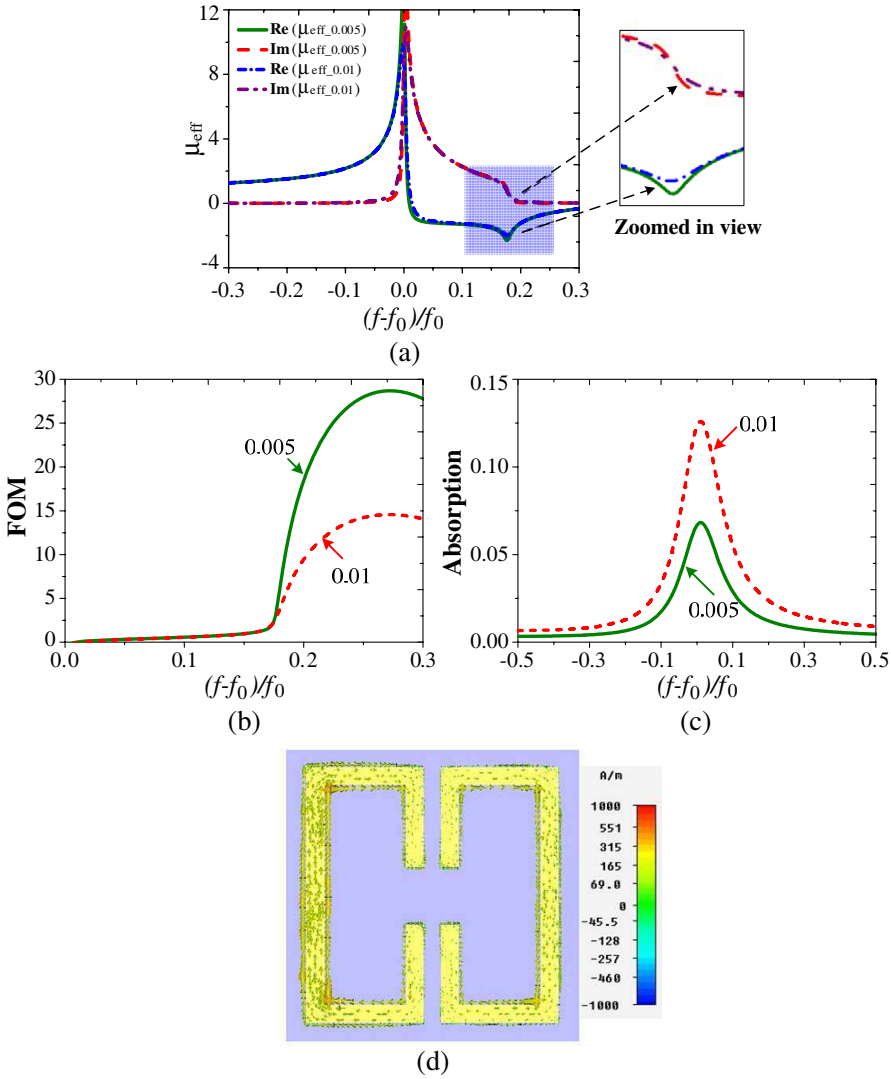

Figure 2. (a) The retrieved results for the real and imaginary parts of the effective permeability of the SRR. (b) The FOMs of the SRR. (c) The absorption losses of the SRR. In panels (a)–(c), the 0.005 (0.01) indicate that the SRR is constructed on the FR4 substrate with a loss tangent of 0.005 (0.01). (d) The surface current distribution for the SRR at the magnetic resonance frequency, the maximal scaling is used.

out that there is a curvature in the real part μ_{eff} near 0.18 on the abscissa, which may result from that the transmission data are very small in magnitude in the resonance band, similar to the results in Refs. [19, 21, 25]. To investigate the influence of the FR4's losses on the SRR, the effective permeability of the SRR constructed on the FR4 substrate with the higher loss tangent of 0.01 is also extracted from the scattering parameters, as shown in Fig. 2(a). From Fig. 2(a), it can be seen that, as the FR4's losses increase, the absolute value of the $\mathrm{Re}(\mu_{eff})$ becomes smaller, and the $\mathrm{Im}(\mu_{eff})$ slightly changes. The figure of merits (FOMs) and the absorption spectra of the SRRs with different FR4's losses are also calculated by using the formulas (1) [37] and (2) [35], and displayed in Figs. 2(b) and (c), respectively.

$$\mathrm{FOM} = \left|\frac{\mathrm{Re}(\mu_{eff})}{\mathrm{Im}(\mu_{eff})}\right| \tag{1}$$

$$A = 1 - |S_{11}|^2 - |S_{21}|^2 \tag{2}$$

From these figures, one can see that the FOM is hardly affected by the losses of the FR4 near the resonance frequency ($(f - f_0)/f_0 < 0.18$), but in a finite bandwidth deviated from the resonance frequency ($0.18 < (f - f_0)/f_0 < 0.3$), the FOM obviously decreases as the FR4'loss tangent increases from 0.005 to 0.01. Meanwhile, the overall absorption loss of the SRR metamaterial enhances.

In order to investigate the generation mechanism of the losses in the SRR, the surface current distribution of the SRR at the magnetic resonance frequency is simulated and shown in Fig. 2(d). It can be seen that the induced current flows annularly along the SRR's arms, which produces the magnetic dipole moment and leads to the negative permeability effect of the SRR. However, we note that the induced current distribution is not uniform. To be specific, the current intensity on the left arm of the SRR is much larger than that on the right arm for the SRR. In this case, accompanying the excitation of the magnetic dipole moment, the electric dipole moment is also excited, which causes large radiation losses. It needs to specially point out that although the magnetic dipole has radiation losses, the radiation losses of the magnetic dipole are much lower than those of the corresponding electric dipole, which is consistent with the view proposed by Ref. [34]. As a result, the magnetic dipole (SRR) with the uniformly distributed current is expected to exhibit the low loss property. Therefore, in order to obtain the low loss SRR, the residual electric dipole moment should be effectively suppressed.

3. REALIZATIONS OF THE ULTRA-LOW LOSS SRR

To suppress the residual electric dipole moment in the unit cell of the SRR, the circular current on the SRR is expected to exhibit the uniform distribution. We demonstrate that such a dramatically decreased the metamaterial loss is achieved by incorporating the lumped and distributed capacitors and the dielectric medium into the existing SRR. Such three arrangements that, as is shown in the following, induce the redistribution of the surface current of the SRR loop and thus suppress the residual electric dipole moment associated with the existing SRR. For simplifying the description of SRRs in the paper, we use throughout the manuscript the abbreviations "SRR-LC" for the SRR with lumped capacitor as shown in Fig. 1(b), the abbreviations "SRR-IDCs" for the SRR with interdigital capacitors (IDCs) as shown in Fig. 1(c), and the abbreviations "SRR-die" for the SRR with dielectric medium as shown in Fig. 1(d).

3.1. SRR-LC

Now, let us consider this arrangement that the lumped capacitor is added to the SRR structure, as shown in Fig. 1(b). The dimensions for the SRR-LC are kept the same as dimensions of the SRR shown in Fig. 1(a). The lumped capacitor value is 1 pF. When the lumped capacitors are incorporated into the SRR structure, the SRR's resonance frequency decreases from 4.63 GHz to 1.74 GHz because of the increase of the totally equivalent capacitor of the SRR, and thus the miniaturization of the SRR is achieved [39, 40]. To demonstrate the validity of the loss reduction of the SRR structure, the effective permeabilities of the SRR and SRR-LC, as functions of the normalized frequency $(f - f_0)/f_0$ (f_0 is the magnetic resonance frequency), are retrieved as shown in Fig. 3(a). It is seen that the imaginary part of the permeability of the SRR-LC approaches 0 faster than the real part of its permeability, and the effective permeability μ_{eff} becomes much stronger and narrower compared to the case without lumped capacitor. These significant features are widely considered as typical signs of the low loss, as pointed out by Refs. [21, 25]. The absorption losses for the SRR and SRR-LC are also calculated. The calculated results are displayed in Fig. 3(b). From Fig. 3(b), we observe that the absorption losses for the SRR-LC are greatly reduced. Moreover, near the resonance frequency, we note that the imaginary part value of the permeability of the SRR-LC is much smaller than the case without lumped capacitor, but the negative permeability effect of the former is far larger than the latter's effect (see the highlight areas shown in Fig. 3(a)). Accordingly, the FOM of the SRR-LC becomes very large,

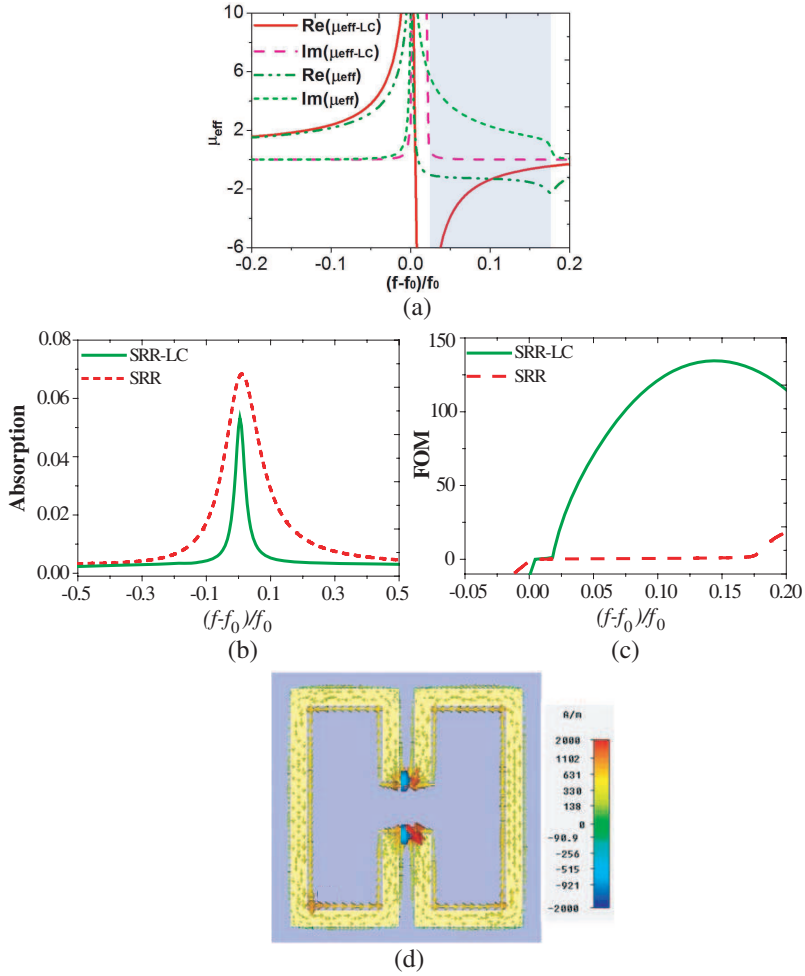

Figure 3. (a) The retrieved results for the real and imaginary parts of the effective permeabilities for the SRR and SRR-LC. (b) The absorption losses of the SRR and SRR-LC. (c) The FOMs of the SRR and SRR-LC. (d) The surface current distribution at the frequency of the magnetic resonance (1.74 GHz) for the SRR-LC, the maximal scaling is used.

approaching values of 140 (see Fig. 3(c)).

To understand the physical mechanism of the loss reduction of the SRR, the surface current distribution at the magnetic resonance frequency (1.74 GHz) is displayed in Fig. 3(d). Noting that the induced current on the SRR loop exhibits the anti-symmetric distribution and

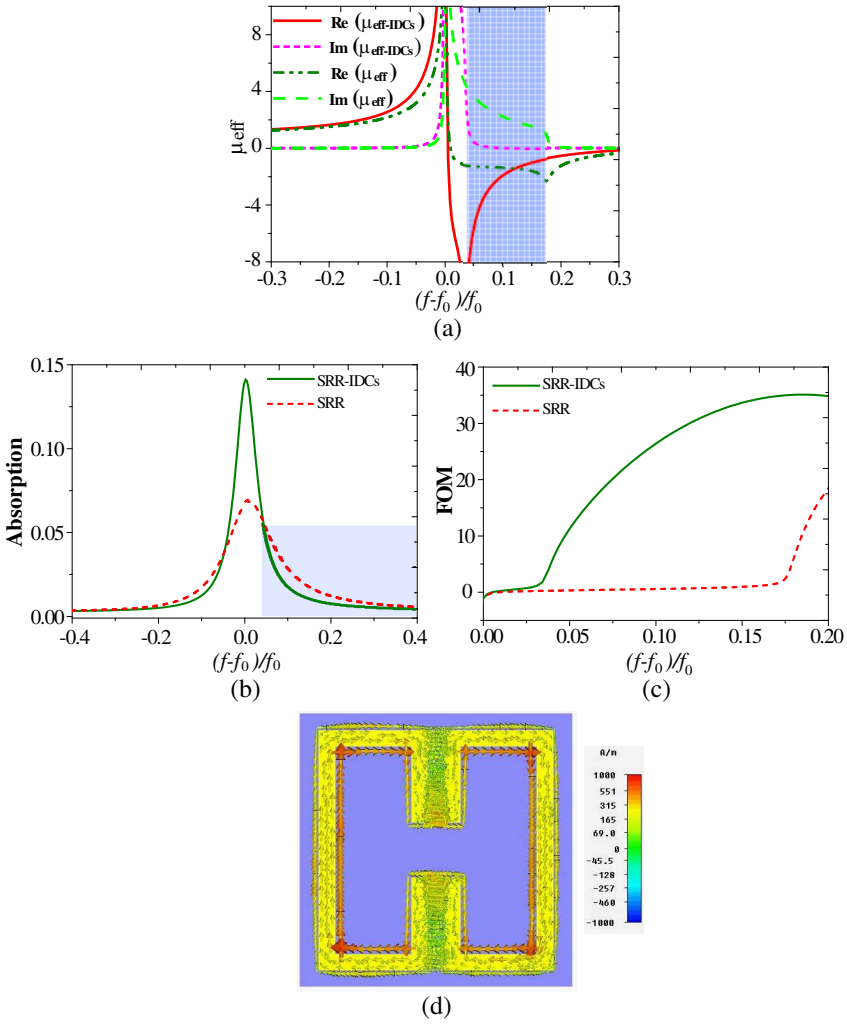

Figure 4. (a) The real and imaginary parts of effective permeabilities for the SRR and SRR-IDCs. (b) The absorption losses of the SRR and SRR-IDCs. (c) The FOMs of the SRR and SRR-IDCs. (d) The surface current distribution at the frequency of the magnetic resonance (2.34 GHz) for the SRR-IDCs, the maximal scaling is used.

the current intensity on left-right arms of the SRR is comparative, which means that there is almost not residual electric dipole moment in the SRR's cell. As a consequence, the radiation loss of the SRR is greatly reduced and the low loss SRR is achieved.

3.2. SRR-IDCs

As discussed above, the lumped capacitor can be incorporated into the SRR structure to suppress the residual electric dipole moment and thus achieve the low loss magnetic metamaterial. However, lumped elements are not available at higher radio frequencies such as millimeter waves because of their distributed parameters. As the counterpart of the lumped capacitor, IDCs have been widely used to design left-handed metamaterials [41, 42] at microwave frequencies. Moreover, IDCs have been used as quasi-lumped elements at higher frequency [43]. In the following, we start to analyze the loss property of the SRR-IDCs (see Fig. 1(c)). The geometric dimensions of the SRR-IDCs are the same as dimensions of the SRR shown in Fig. 1(a). When the IDCs are integrated with the SRR structure, the SRR's resonance frequency decreases from 4.63 GHz to 2.34 GHz because of the increased equivalent capacitor of the SRR, and thus the miniaturization of the SRR structure is achieved [39, 40]. The effective permeability, absorption loss and FOM of the SRR-IDCs as functions of the normalized frequency are displayed in Figs. 4(a)–(c). For the purpose of comparison, the effective permeability, the absorption loss and the FOM of the independent SRR are also included. Similar to the simulated results for the SRR-LC, the weak and broad μ_{eff} becomes stronger and narrower after the introduction of IDCs for the SRR metamaterial. Accordingly, the FOM of the SRR-IDCs increases, approaching values of 40. Meanwhile, we note that although the IDCs introduce additional losses for the SRR near the magnetic resonance frequency, the losses for the SRR are reduced in a finite bandwidth deviated from the resonance frequency (see the highlight areas shown in Fig. 4(b)). The surface current distribution of the SRR-IDCs at the magnetic resonance frequency (2.34 GHz) is also displayed to further demonstrate the suppressing degree of the radiation loss (see Fig. 4(d)). It is obviously seen that the uniform current distributes on the SRR loop and there is almost not residual electric dipole moment in the SRR's unit cell contributing to radiation losses. Thus, the low loss magnetic metamaterial is achieved by using the SRR-IDCs.

3.3. SRR-die

It needs to specially point out that our proposed method is also valid at THz frequencies and in the optical regime. As shown in following, the validity of losses reduction of the SRR-die (see Fig. 1(d)) is examined. In this case, the role of the dielectric medium in the SRR metamaterial is comparative to the role of the lumped capacitor and IDCs in the microwave regime. When the dielectric

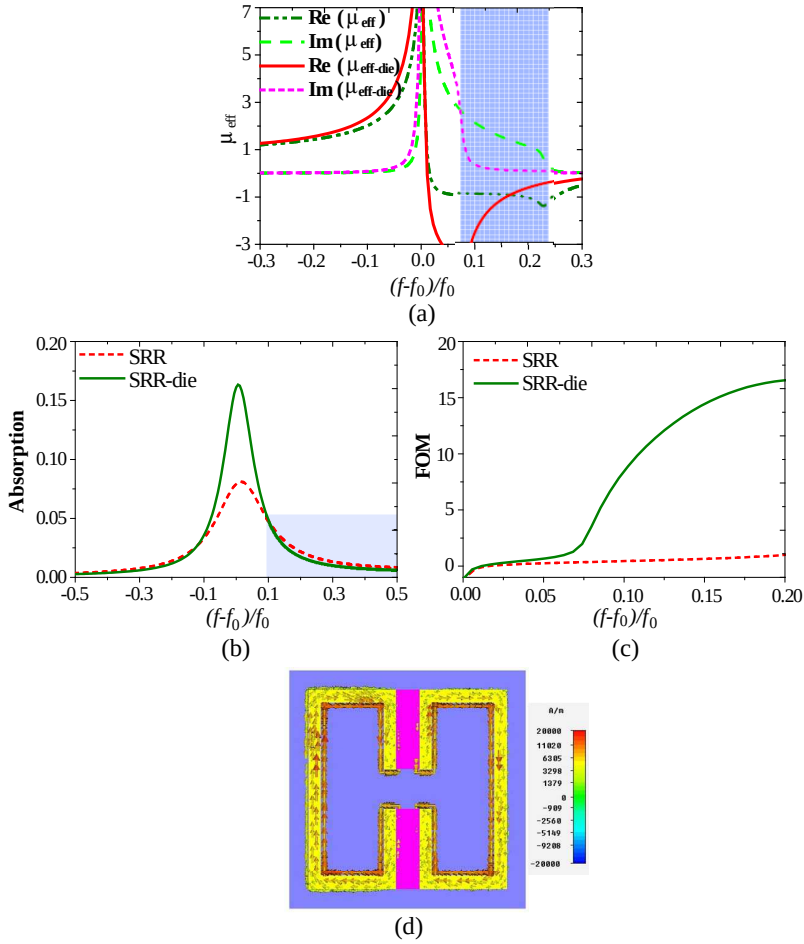

Figure 5. (a) The real and imaginary parts of effective permeabilities for the SRR and SRR-die. (b) The absorption losses of the SRR and SRR-die. (c) The FOMs of the SRR and SRR-die. (d) The surface current distribution at 0.34 THz for the SRR-die, the maximal scaling is used.

mediums are added to the SRR structure, the SRR's resonance frequency decreases from 0.52 THz to 0.34 THz because of the increased equivalent capacitor of the SRR, and thus the miniaturization of the SRR structure is achieved [39, 40]. Similar to the microwave frequencies, the negative permeability effect becomes stronger and narrower after the introduction of the dielectric medium for the SRR metamaterial, as revealed in Fig. 5(a). Accordingly, the FOM increases

from 0.2 to 16 and the absorption losses are reduced in a finite bandwidth deviated from the resonance frequency (see Figs. 5(b)–(c)). The surface current distribution at the magnetic resonance frequency (0.34 THz) is plotted in Fig. 5(d). From Fig. 5(d), we can see that the uniform current flows around the SRR loop, which further demonstrates that the residual electric dipole moment in the SRR's cell is effectively suppressed and the radiation losses of the SRR are greatly reduced. Thus, the SRR-die exhibits the low loss property at THz frequencies. The results of our study provide useful guidelines for the design and engineering of negative index metamaterials with low loss at THz frequencies.

4. CONCLUSION

In this paper, we propose an effective way to tremendously reduce the losses of the SRR by suppressing the residual electric dipole moment. We start to discuss on the analysis of the loss mechanism of the SRR. Note that the residual electric dipole moment on the SRR loop leads to the high radiation losses. In order to obtain the ultra-low loss SRR metamaterial, three different schemes are applied in the numerical simulations and the validities of their corresponding loss reductions are studied by calculating the effective permeability, absorption loss, FOM and surface current. Simulation results indicate that the SRRs integrated with the lumped capacitor, IDCs and dielectric medium show the low loss property in a finite bandwidth deviated from the resonance frequency owing to suppression of the residual electric dipole moment. Furthermore, their FOMs are greatly increased compared to the case of the independent SRR and the uniformly distributed currents on the SRR loop can be observed, which further verifies the ultra-low loss property of the SRR metamaterial. The result of our study proposes another way to realize the negative permeability metamaterial with low loss at microwave and THz frequencies, and it opens up new prospects for studies of the unique electromagnetic effects associated with negative and zero index materials such as superlens, reversed Doppler effects, and electromagnetic cloaks.

ACKNOWLEDGMENT

This work is supported by the Fundamental Research Funds for the Central Universities (Grand No. HIT. IBRSEM. 201122), and the National Natural ScienceFoundation of China (Grant Nos. 60801015 and 60971064), and a grant from the Ph.D. Programs Foundation of Ministry of Education of China (No. 20092302110030).

REFERENCES

1. Pendry, J. B., "Negative refraction makes a perfect lens," *Physical Review Letters*, Vol. 85, 3966–3969, 2000.
2. Schurig, D., J. J. Mock, B. J. Justice, S. A. Cummer, J. B. Pendry, A. F. Starr, and D. R. Smith, "Metamaterial electromagnetic cloak at microwave frequencies," *Science*, Vol. 314, 977–980, 2006.
3. Liu, S.-H. and L.-X. Guo, "Negative refraction in an anisotropic metamaterial with a rotation angle between the principal axis and the planar interface," *Progress In Electromagnetics Research*, Vol. 115, 243–257, 2011.
4. Meng, F.-Y., Y.-L. Li, K. Zhang, Q. Wu, and J. L.-W. Li, "A detached zero index metamaterial lens for antenna gain enhancement," *Progress In Electromagnetics Research*, Vol. 132, 463–478, 2012.
5. Burlak, G., "Spectrum of cherenkov radiation in dispersive metamaterials with negative refraction index," *Progress In Electromagnetics Research*, Vol. 132, 149–158, 2012
6. Li, J., F.-Q. Yang, and J. Dong, "Design and simulation of L-shaped chiral negative refractive index structure," *Progress In Electromagnetics Research*, Vol. 116, 395–408, 2011.
7. Shao, J., H. Zhang, Y. Lin, and H. Xin, "Dual-frequency electromagnetic cloaks enabled by LC-based metamaterial circuits," *Progress In Electromagnetics Research*, Vol. 119, 225–237, 2011.
8. He, X.-J., Y. Wang, J.-M. Wang, and T.-L. Gui, "Dual-band terahertz metamaterial absorber with polarization insensitivity and wide incident angle," *Progress In Electromagnetics Research*, Vol. 115, 381–397, 2011.
9. Faruque, M. R. I., M. T. Islam, and N. Misran, "Design analysis of new metamaterial for EM absorption reduction," *Progress In Electromagnetics Research*, Vol. 124, 119–135, 2012.
10. Sabah, C. and H. G. Roskos, "Design of a terahertz polarization rotator based on a periodic sequence of chiral-metamaterial and dielectric slabs," *Progress In Electromagnetics Research*, Vol. 124, 301–314, 2012.
11. Xie, Y., J. Jiang, and S. He, "Proposal of cylindrical rolled-up metamaterial lenses for magnetic resonance imaging application and preliminary experimental demonstration," *Progress In Electromagnetics Research*, Vol. 124, 151–162, 2012.
12. Zarifi, D., H. Oraizi, and M. Soleimani, "Improved performance of circularly polarized antenna using semi-planar chiral metamaterial

covers," *Progress In Electromagnetics Research*, Vol. 123, 337–354, 2012.

13. Chen, H., L. Huang, X. Cheng, and H. Wang, "Magnetic properties of metamaterial composed of closed rings," *Progress In Electromagnetics Research*, Vol. 115, 317–326, 2011.
14. Huang, L. and H. Chen, "Multi-band and polarization insensitive metamaterial absorber," *Progress In Electromagnetics Research*, Vol. 113, 103–110, 2011.
15. Kuznetsov, S. A., A. G. Paulish, A. V. Gelfand, A. Lazorskiy, and V. N. Fedorinin, "Matrix structure of metamaterial absorbers for multispectral terahertz imaging," *Progress In Electromagnetics Research*, Vol. 122, 93–103, 2012.
16. Veselago, V. G., "The electrodynamics of substances with simultaneously negative values of ε and μ," *Soviet Physics Uspekhi*, Vol. 10, 509–514, 1968.
17. Pendry, J. B., A. J. Holden, D. J. Robbins, and W. J. Stewart, "Magnetism from conductors and enhanced non-linear phenomena," *IEEE Transactions on Microwave Theory and Techniques*, Vol. 47, 2075–2084, 1999.
18. Smith, D. R., W. J. Padilla, D. C. Vier, S. C. Nemat-Nasser, and S. Schultz, "Composite media with simultaneously negative permeability and permittivity," *Physical Review Letters*, Vol. 84, 4184–4187, 2000.
19. Zhou, X., Y. H. Liu, and X. Zhao, "Low losses left-handed materials with optimized electric and magnetic resonance," *Applied Physics A*, Vol. 98, 643–649, 2010.
20. García-Meca, C., R. Ortuño, R. Salvador, A. Martínez, and J. Martí, "Low-loss single-layer metamaterial with negative index of refraction at visible wavelengths," *Optics Express*, Vol. 15, 9320–9325, 2007.
21. Zhou, J., Th. Koschny, and C. M. Soukoulis, "An efficient way to reduce losses of left-handed metamaterials," *Optics Express*, Vol. 16, 11147–11152, 2008.
22. Zhao, Y. X., F. Chen, Q. Shen, Q. W. Liu, and L. M. Zhang, "Optimizing low loss negative index metamaterial for visible spectrum using differential evolution," *Optics Express*, Vol. 19, 11605–11614, 2011.
23. Bossard, J. A., S. Yun, D. H. Werner, and T. S. Mayer, "Synthesizing low loss negative index metamaterial stacks for the mid-infrared using genetic algorithms," *Optics Express*, Vol. 17, 14771–14779, 2009.

24. Bratkovsky, A., E. Ponizovskaya, S.-Y. Wang, P. Holmstrm, L. Thylén, Y. Fu, and H. Ågren, "A metal-wire/quantum-dot composite metamaterial with negative ε and compensated optical loss," *Applied Physics Letters*, Vol. 93, 193106, 2008.
25. Fang, A., Z. X. Huang, T. Koschny, and C. M. Soukoulis, "Overcoming the losses of a split ring resonator array with gain," *Optics Express*, Vol. 19, 12688–12699, 2011.
26. Shen, J.-Q., "Gain-assisted negative refractive index in a quantum coherent medium," *Progress In Electromagnetics Research*, Vol. 133, 37–51, 2013.
27. Tassin, L. Zhang, T. Koschny, E. N. Economou, and C. M. Soukoulis, "Low loss metamaterials based on classical electromagnetically induced transparency," *Physical Review Letters*, Vol. 102, 051901, 2009.
28. Zhu, L., F. Y. Meng, J. H. Fu, and Q. Wu, "Electromagnetically induced transparency metamaterial with polarization insensitivity based on multi-quasi-dark modes," *Journal of Physics D: Applied Physics*, Vol. 45, 445105, 2012.
29. Zhu, L., F. Y. Meng, J. H. Fu, Q. Wu, and J. Hua, "An approach to configure low-loss and full transmission metamaterial based on electromagnetically induced transparency," *IEEE Transactions on Magnetics*, Vol. 48, 4285–4288, 2012.
30. Liu, N., L. Langguth, T. Weiss, J. Kästel, M. Fleischhauer, T. Pfau, and H. Giessen, "Plasmonic analogue of electromagnetically induced transparency at the drude damping limit," *Nature Materials*, Vol. 8, 758–762, 2009.
31. Zhu, L., F. Y. Meng, J. H. Fu, Q. Wu, and J. Hua, "Multi-band slow light metamaterial," *Optics Express*, Vol. 20, 4494–4502, 2012.
32. Zhu, L., L. Dong, F. Y. Meng, J. H. Fu, and Q. Wu, "Influence of symmetry breaking in a planar metamaterial on transparency effect and sensing application," *Applied Optics*, Vol. 51, 7794–7799, 2012.
33. Meng, F. Y., F. Zhang, K. Zhang, and Q. Wu, "Low-loss magnetic metamaterial based on analog of electromagnetically induced transparency," *IEEE Transactions on Magnetics*, Vol. 47, 3347–3350, 2011.
34. Li, T. Q., H. Liu, T. Li, S. M. Wang, J. X. Cao, Z. H. Zhu, Z. G. Dong, S. N. Zhu, and X. Zhang, "Suppression of radiation loss by hybridization effect in two coupled split-ring resonators," *Physical Review B*, Vol. 80, 115113, 2009.

35. Meng, F. Y., J. H. Fu, K. Zhang, Q. Wu, J. Y. Kim, J. J. Choi, B. Lee, and J. C. Lee, "Metamaterial analogue of electromagnetically induced transparency in two orthogonal directions," *Journal of Physics D: Applied Physics*, Vol. 44, 265402, 2011.
36. Papasimakis, N., V. A. Fedotov, N. I. Zheludev, and S. L. Prosvirnin, "Metamaterial analog of electromagnetically induced transparency," *Physical Review Letters*, Vol. 101, 253903, 2008.
37. Tsakmakidis, K. L., M. S. Wartak, J. J. H. Cook, J. M. Hamm, and O. Hess, "Negative-permeability electromagnetically induced transparent and magnetically active metamaterials," *Physical Review B*, Vol. 81, 195128, 2010.
38. Szabó, Z., G.-H. Park, R. Hedge, and E. Li, "A unique extraction of metamaterial parameters based on Kramers-Kronig relationship," *IEEE Transactions on Microwave Theory and Techniques*, Vol. 58, 2646–2653, 2010.
39. Erentok, A., R. W. Ziolkowski, J. A. Nielsen, R. B. Greegor, C. G. Parazzoli, et al., "Low frequency lumped element-based negative index metamaterial," *Applied Physics Letters*, Vol. 91, 184104, 2007.
40. Ban, Y.-L., J.-H. Chen, S.-C. Sun, J. L.-W. Li, and J.-H. Guo, "Printed wideband antenna with chip-capacitor-loaded inductive strip for LTE/GSM/UMTS WWAN wireless USB dongle applications," *Progress In Electromagnetics Research*, Vol. 128, 313–329, 2012.
41. Lai, A., T. Itoh, and C. Caloz, "Composite right/left-handed transmission line metamaterials," *IEEE Microwave Magazine*, Vol. 5, 3450, 2004.
42. Gil, M., J. Bonache, J. Garcia-Garcia, J. Martel, and F. Martin, "Composite right/left-handed metamaterial transmission lines based on complementary split-rings resonators and their applications to very wideband and compact filter design," *IEEE Transactions on Microwave Theory and Techniques*, Vol. 55, 1296–1304, 2007.
43. Alley, G. D., "Interdigital capacitors and their application to lumped element microwave integrated circuits," *IEEE Transactions on Microwave Theory and Techniques*, Vol. 18, 1028–1033, 1970.